Journal of Nuclear Materials 377 (2008) 147–154

Contents lists available at ScienceDirect

Journal of Nuclear Materials

journal homepage: www.elsevier.com/locate/jnucmat

Effect of Cr on the mechanical properties and microstructure of Fe–Cr model alloys after n-irradiation

M. Matijasevic, A. Almazouzi *

SCK·CEN, Nuclear Materials Sciences Institute, Boeretang 200, 2400 Mol, Belgium

A B S T R A C T

High-chromium ferritic–martensitic steels are candidate structural materials for high-temperature applications in fusion reactors and accelerator driven systems (ADS). Cr concentration has been shown to be a key parameter which needs to be optimized in order to guarantee the best corrosion and swelling resistance, together with the minimum embrittlement. The behavior of Fe–Cr model alloys with different Cr concentrations (0, 2.5, 5, 9 and 12 wt%Cr) has been studied. Tensile tests have been performed in order to characterize the flow properties in the temperature range from −160 °C to 300 °C. The trend of the yield strength with temperature shows that the strain hardening is the same for all materials at low temperatures, even though they have different microstructures. The same materials have been neutron-irradiated at 300 °C in the BR2 reactor of SCK·CEN, up to three different doses (0.06, 0.6 and 1.5 dpa). The results obtained so far indicate that even at these low doses, the Cr content affects the hardening behavior of Fe–Cr binary alloys. Using the Orowan mechanism, the TEM observed microstructure provides an explanation of the obtained hardening but only at the very low dose, 0.06 dpa. At higher doses, other hardening mechanisms are needed.

© 2008 Elsevier B.V. All rights reserved.

1. Introduction

High-chromium (9–12 wt%) ferritic/martensitic steels are candidates as potential first-wall and breeding blanket structural materials for future fusion reactors [1] as well as for fuel cladding and the spallation target in the accelerator driven systems [2]. Their use for these applications requires a careful assessment of their mechanical stability under high energy neutron irradiation [3] and their compatibility with the cooling media [4]. Thus, their chemical composition and thermo-mechanical treatments have been optimized over decades of experimental investigations to resist the expected harsh conditions. Indeed, it was found that the steels containing 9 wt% Cr are resistant to swelling [5], less brittle [6] and reasonably immune to erosion corrosion [7] in the temperature range of 300–500 °C. The physical understanding of these empirical findings is the aim of this investigation.

Although Cr-steels became very popular just after World War I, as the consequence of the scarcity of Tungsten [8]. Already in the 1940s, it was established that the behavior of the binary alloy Fe–Cr depends strongly on Cr content in terms of magnetic behavior and electrical resistivity [9]. It is, however, only very recently that the effect of Cr on the mixing enthalpy of the alloys [10] and on their resistance to swelling have been elucidated theoretically [11]. Furthermore, the effect of Cr and temperature on defect accumulation was studied for some time [12–16]. As described by Yoshida et al. [12], dislocation loops nucleate and grow slowly under irradiation, especially at lower temperatures. At higher temperatures loops are larger and their density decreases. In the presence of Cr they nucleate and grow faster and with increasing temperature their density decreases while their size increases. Cr has a strong effect on defect stability. Thus, while in Fe defects start shrinking or disappearing at $T > 750$ K, when adding Cr, the shrinkage and the motion of the observed loops are significantly suppressed [14]. However, the effect of Cr concentration on the microstructural changes and their influence on the mechanical behavior has never been studied thoroughly.

The general objective of this work is to investigate the effect of Cr on the irradiation-induced defect formation and accumulation in Fe–Cr based model alloys with well defined chemical compositions and microstructures both to examine the microstructure changes and the hardening induced by well controlled neutron irradiation and also to help the theoreticians to bench-mark their codes.

In this paper, the properties of the investigated materials will be described in Section 2. In Section 3, the microstructural changes due to neutron irradiation are described in detail. The tensile data obtained are summarized in Section 4 and finally the relationship between the microstructures and the hardening of the investigated four binary alloys, are discussed in terms of Orowan mechanism.

* Corresponding author. Tel.: +32 14 33 3096; fax: +32 14 32 1216.
E-mail address: aalmazou@SCKCEN.be (A. Almazouzi).

0022-3115/$ - see front matter © 2008 Elsevier B.V. All rights reserved.
doi:10.1016/j.jnucmat.2008.02.061

2. Materials

The investigated materials have been laboratory-fabricated, thermo-mechanically treated and thoroughly analyzed in terms of microstructure and tensile properties.

2.1. Composition and heat treatment

The materials used in this work were Fe–Cr based model alloys with 2.5%Cr (2.36 wt% Cr), 5%Cr (4.62 wt%Cr), 9%Cr (8.39 wt%Cr) and 12%Cr (11.62 wt%Cr) obtained by furnace melting of industrial pure Fe and Cr. After casting, the obtained ingots were cold worked under protective atmosphere to fabricate plates of 9 mm in thickness. Similar to the standard practice of ferritic–martensitic steels, Fe–Cr model alloys were treated at 1050 °C, for 1 h in high vacuum for austenisation and stabilization. Thereafter, the tempering was done at 730 °C for 4 h, followed by air cooling. The final product was chemically analyzed using the adequate techniques to measure both substitutional and interstitial impurities. The total amount of impurities did not exceed 300 wt ppm [17] as reported in Table 1.

2.2. Electrical resistivity

Electrical resistivity measurements were performed between liquid helium temperature (4.2 K) and room temperature (300 K) with and without a saturated longitudinal magnetic field of 0.5 T. The measured resistivities (μΩ cm) obtained as a function of Cr content at the lowest (full symbols) and the highest (open symbols) temperatures are shown in Fig. 1, together with those found in the literature for binary Fe–Cr alloys. It should be mentioned here that the magnetic field had no effect on the measured resistivity in the investigated alloys (therefore, the results obtained with, are omitted here for figure clarity). In the figure, the values of the resistivity obtained by using the empirical model proposed by Maury et al. [18] are also reported. As it can be noticed, the results obtained here are very comparable to those reported in earlier investigations [18–20]. In fact, one can distinguish clearly two domains: below and above 9%Cr. This variation is believed to be one of the reasons affecting the response of this system after irradiation as well. The absolute values found here are of the same order of magnitude as those reported in the literature [18–20] demonstrating that the investigated alloys can be considered as binary systems with negligible amount of interstitial (N, C) impurities.

2.3. Microstructure for non-irradiated material

Specimens of 3 mm diameter that were first cut by an EDM machine with a diameter of 1 mm, fine mechanically polished to about 100 mm, were then prepared using the conventional jet polishing technique and examined using a TEM (JOEL 3010 EX) with an acceleration voltage of 300 KeV. The microstructure of the as-prepared Fe–Cr model alloys is illustrated by the images in Fig. 2. It can be seen that with increase of Cr content, the microstructure

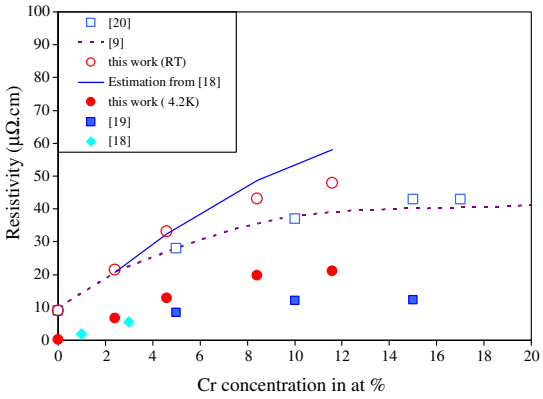

Fig. 1. Electrical resistivity of Fe–Cr binary alloys. The low temperature (full symbols) and the room temperature (open symbols) obtained without magnetic field are compared with those reported in the literature [18–20].

is changing from fully ferritic to ferrite and bainite. Thus, TEM bright field images of Fe–2.5%Cr and Fe–5%Cr alloys show massive amount of ferrite grains with randomly oriented grain boundaries that are the signature of fast cooling which prevents the formation of equiaxed ferrite. The dislocation density for these two alloys is respectively 1.2×10^9 and 5.8×10^9 cm^{-2}. High Cr alloys with 9% and 12%Cr content, have very small grains of the order of 1 μm. Their microstructure consists of bainitic ferrite which is obtained by rapid cooling. Grains are small with many planar boundary segments. The density of dislocations for Fe–9%Cr is 6.3×10^9 cm^{-2} and for Fe–12%Cr a value of 5.5×10^9 cm^{-2} is obtained. Dislocations are predominately of type $a_0/2\langle 1\,1\,1\rangle$ Burgers vectors, where a_0 is the lattice parameter. Thus, the microstructure of high Cr alloys is considered to be very similar to the usual ferritic–martensitic steels [21], as the grains are pretty similar to the martensitic laths, but in these model alloys the laths consist of ferrite grains with a well structured density of dislocations.

2.4. Tensile tests of as-received model alloys

The tensile specimens with nominal dimensions (overall length = 27 mm, gage length = 12 mm and diameter = 2.4 mm) were prepared using an EDM cutting machine followed by a fine mechanical polishing of the surface. Tensile tests were performed according to ASTM E8M-01 and E21-92 (1998) standards with an electro-mechanical test frame (INSTRON 8500, model 1362), and a crosshead displacement rate of 0.2 mm/min corresponding to a strain rate of approximately 2.8×10^{-4} s^{-1} in the temperature range from −160 °C to 300 °C. Engineering stress–strain curves at room temperature (RT) are presented in Fig. 3. Both the yield stress (YS) and the ultimate tensile stress (UTS) for model alloys increase linearly with Cr content. In terms of ductility, low Cr alloys are more ductile than high Cr alloys. It was found that the ductility of the investigated materials is also related to the grain size. Thus, low Cr alloys that have larger grain sizes tend to have a lower

Table 1
Chemical composition of investigated Fe–Cr model alloys measured in wt% Fe balance the alloys of reference 251, 259, 252, 253 are named Fe–2.5Cr, Fe–5Cr, Fe–9Cr, Fe–12Cr, respectively in the text

Alloy	Mn	Si	P	S	Al	Ti	Cr	Ni	O	C	N	V	Total amount of impurity (wt ppm)
251	0.009	0.02	0.013	0.0020	0.003	0.004	2.4	0.044	0.035	0.008	0.0117	0.001	~149
259	0.02	0.04	0.011	0.006	0.0033	0.0028	4.6	0.06	0.065	0.02	0.0127	0.001	242
252	0.03	0.09	0.012	0.00066	0.0069	0.0034	8.4	0.07	0.066	0.02	0.0148	0.002	333
253	0.03	0.11	0.05	0.006	0.003	0.0037	11.6	0.09	0.03	0.027	0.0237	0.002	~375

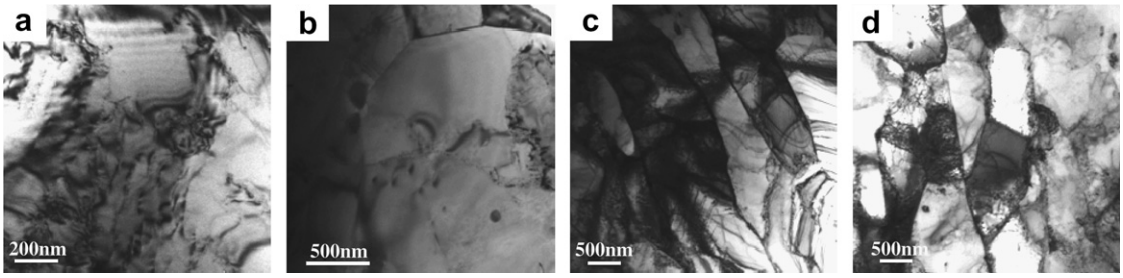

Fig. 2. TEM bright field images showing the grain size evolution of Fe–Cr model alloys, with increasing Cr concentration 2.5Cr (a), 5Cr (b), 9Cr (c) and 12Cr (d).

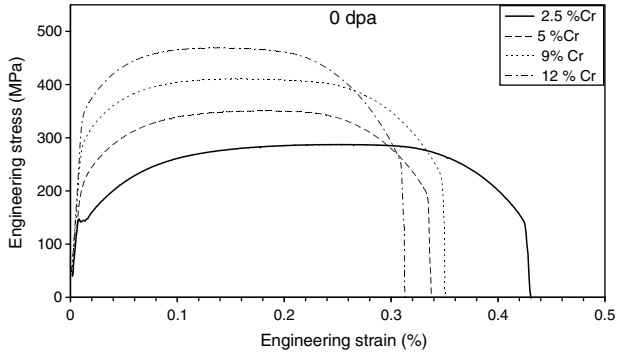

Fig. 3. Engineering stress and strain curves at RT of the model alloys before irradiation.

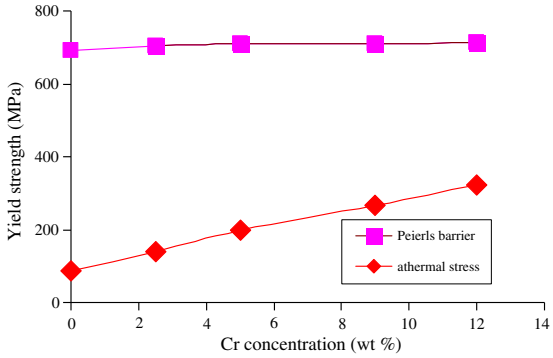

Fig. 5. Peierls stress, τ_p, and athermal stress, σ_{ath}, dependence with Cr concentration for un-irradiated FeCr alloys.

toughness than high Cr alloys having smaller grains. The yield strength dependence on temperature is shown in Fig. 4. The obtained values of yield strength have been fitted as a function of test temperature using the general formula proposed by Dieter [22]:

$$\sigma_{0.2} = \sigma_{ath} + \sigma_0 e^{-\beta T}, \quad (1)$$

where $\sigma_{0.2}$ is the yield strength, and σ_{ath}, σ_0 and β are regression coefficients. In particular, σ_{ath} represents the athermal component. It is found that, (i) the athermal stresses increase with Cr concentration due to the pure solution hardening; (ii) σ_0 and β are constants and equal to 40 MPa and 0.013, respectively, for all investigated materials. Peierls stress (τ_p) formulation is given by the following equation [22]:

$$\tau_p = 2\mu/(1-\nu)\exp[-2\pi a/(1-\nu)b], \quad (2)$$

where μ is the shear modulus, ν is the Poisson ratio, a is the distance between slip planes and b is the Burgers vector.

Lattice parameter calculations with respect to Cr concentration yield almost the same results for the lattice parameter $a_0 \sim 2.8$ A, where $a = a_0\sqrt{2}/2$ [10]. Using the values of μ and ν given in [20], the calculated Peierls stress, as the shear stress required to move a dislocation through a crystal is equal to 678 MPa for all model alloys as can be seen in Fig. 5.

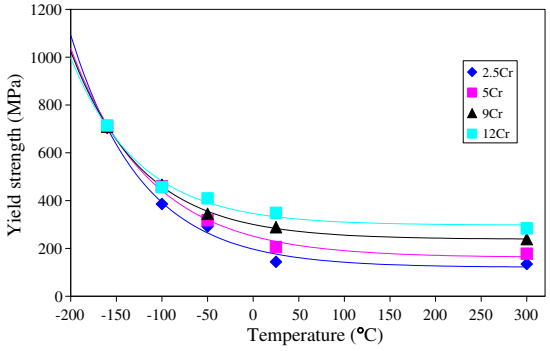

Fig. 4. Yield strength vs temperature.

2.5. Irradiation

Charpy, tensile and TEM samples were thereafter fabricated mostly with the long dimension parallel to the cold rolling direction. Neutron irradiation in reactor BR2 was performed in a dedicated capsule 'MIRE-CR' within the well known CALLISTO-loop [23] equipped with 10 thermocouples to control the temperature during the experiment. The temperature was set to (300 ± 5) °C. The neutron spectrum, fluxes and fluencies experienced by the specimens in their actual location are determined by the power of BR2 and the duration of the irradiation cycles and are calculated by the code GEXBR2-TRPT3 [23]. Dosimeters (Fe foils) have been inserted all along the capsules to allow the determination of the dose. For the determination of the doses, the specific chemical nature of the alloys was not taken into account. Thus, three different doses were reached namely 0.06, 0.6 and 1.5 dpa with a neutron flux of 9×10^{13} n/(cm^2 s) with energy higher than 1 MeV [24]. The variation of the doses found within the same capsule is about 10%.

3. Irradiated material

The investigation of the irradiated samples was performed in the hot cell area using if not the same instrument as in the case of the microstructure, testing machines that are well calibrated and equipped with the same acquisition systems as those used for un-irradiated materials. It should be noted at this point that, several tests have been performed for the un-irradiated samples but only one or two tensile tests were performed with irradiated specimens due to their limited number.

3.1. Microstructure

Irradiation-induced microstructure changes and defects have been studied by TEM. For this purpose, samples of 3 mm diameter and 0.3 mm thickness were prepared before irradiation. The post irradiation examination consists of preparing TEM specimens using the conventional method (mechanical polishing followed by chemical etching) in a protected environment. Thereafter, weak beam dark field (g, $4g$) imaging was used for the full characterization of the microstructure. TEM observation for all investigated materials shows rather small defects induced by irradiation. Fig. 6 shows the irradiation-induced microstructure for the Fe–9%Cr model alloys and how it changes with increasing dose from 0.06 to 1.5 dpa. All observed grains are oriented close to a $\{1\,1\,1\}$ zone, and the images were taken with different $g(1\,1\,0)$ type diffraction vectors as indicated on the TEM micrographs. The small white and black spots, which can be seen in all three dark field images, are radiation-induced defect clusters. It was found that these clusters are mostly formed and associated with the dislocation lines in all three specimens. At the lowest dose of 0.06 dpa (see Fig. 6(a)) only a few of them are in the matrix. This specimen was observed in $g(1\,1\,0)$ direction. Although it cannot be excluded that many smaller defects are present but not visible by TEM, the average size is determined from the fitting of a Gaussian distribution to the observed one. Thus, it is found that the average size of defects at this dose is around 5 nm and the density of the defect clusters was determined to be about $1.3 \times 10^{21}/m^3$. At higher doses, it was observed that the size of cluster loops increases with dose. At 0.6 dpa (see Fig. 6(b)) it can observed that the density of defect clusters is higher and defects (imaged as white spots) are present in the matrix as well, as near dislocation lines. The average size is around 7 nm for this middle dose of irradiation. The defect density is about $1.9 \times 10^{21}/m^3$. The defect cluster density in specimens irradiated to higher doses (e. g. 1.5 dpa) seems to decrease. Thus, the observed defect clusters (loops) with average size of 13 nm have a density of $1.7 \times 10^{21}/m^3$ and are located near the initial dislocation network mostly. Decorated dislocation segments at this highest dose are shown in representative micrographs with $g(\bar{1}\,1\,0)$ direction, for Fe–9%Cr alloys in Fig. 6(c). Weak beam contrast using three different orientations have been used to get information on the loop Burgers vectors [25]. This experiment demonstrates that two types of loops are present with $b = a\langle 1\,0\,0\rangle$ and $b = a/2\langle 1\,1\,1\rangle$. The number of loops present is not sufficient to accurately characterize the relative fraction of $\langle 1\,0\,0\rangle$ and $\langle 1\,1\,1\rangle$ loops. Subsequently the effect of Cr concentration on the defect cluster (or dislocation loops) creation was studied.

Fig. 7 presents bright field images of model alloys with increasing Cr concentration at the same irradiation dose of 0.6 dpa. In Fig. 7(a), the microstructure of the Fe–2.5%Cr alloy is shown. Defect clusters are larger compared to higher Cr alloys. Their average size is 13 nm and the density is about $2.6 \times 10^{21}/m^3$. Again all grains are oriented close to a $\langle 1\,1\,1\rangle$ zone and $\{1\,1\,0\}$ type of diffraction vectors have been used. The microstructure of the lowest Cr concentration alloy is very similar to that observed for Fe irradiated to a similar dose and at the same temperature in BR2 [26]. With increasing Cr content, the density of defect clusters decreases and they become smaller. The result for the Fe–5%Cr alloy is shown in Fig. 7(b). The defect density in this alloy is about $2.3 \times 10^{21}/m^3$, while the average size at this middle dose is around 7 nm. Furthermore, it was observed that in the high Cr alloys defect clusters are

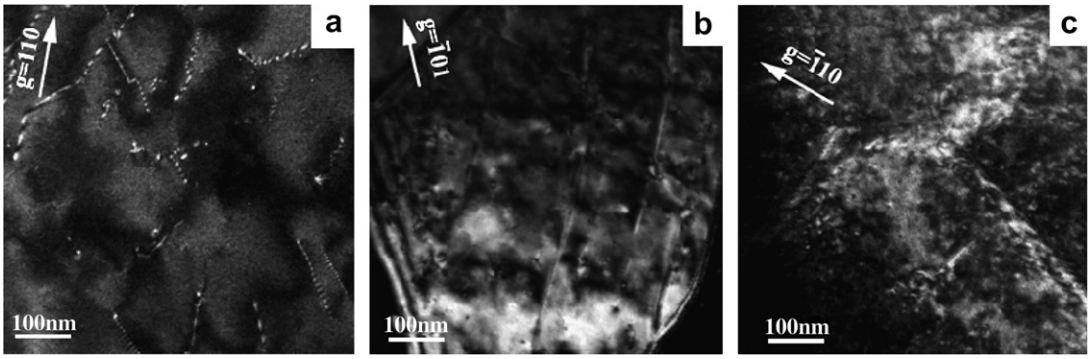

Fig. 6. Dark field TEM micrographs of Fe–9Cr alloy at (a) 0.06 dpa, (b) 0.6 dpa and (c) 1.5 dpa.

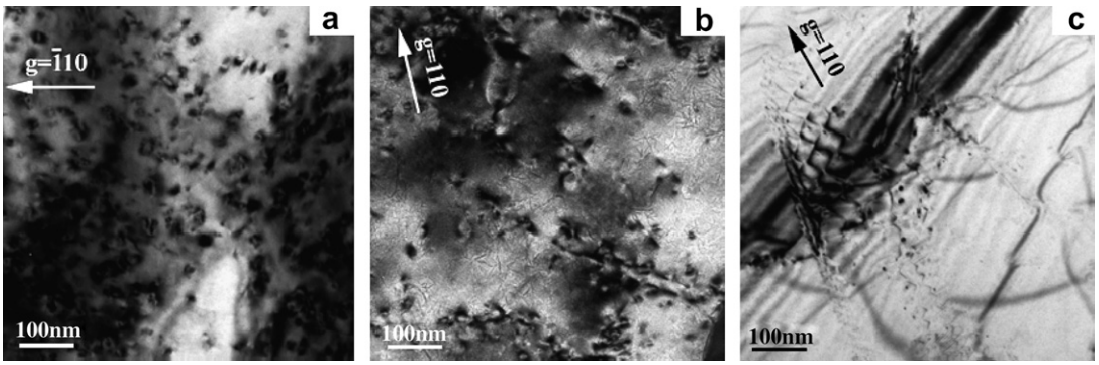

Fig. 7. Bright field TEM micrographs showing the effect of the increase of Cr concentration on the dislocation loop formation at 0.6 dpa (a) Fe–2.5Cr, (b) Fe–5Cr and (c) Fe–12Cr alloys.

located more around the initial dislocations lines than in the matrix as compared with low Cr alloys, where the clusters are quite big and well distributed in matrix. Fig. 7(c) shows a micrograph of the Fe–12%Cr alloy. The average size of the loops for this alloy is around 6 nm, and the defect density is about $1.6 \times 10^{21}/m^3$.

The results of the defect density and loop size measurements vs dose for all Fe–Cr alloys are summarized in Table 2 and illustrated in Fig. 8. In the latter, the full symbols in the graph refer to the defect density and the values are indicated on the left *Y*-axis. It shows how the defect density decreases with increasing Cr concentration and that a maximal density is reached at a dose of 0.6 dpa. The open symbols refer to the loop size and the values are shown on the right *Y*-axis. The results obtained by Hernández-Mayoral [27] who examined pure Fe by TEM after irradiation under similar conditions as the present work, namely in BR2 reactor, at 300 °C but a slightly different neutron flux are also added to the figure for comparison. It can be seen from the figure that at low doses there is no major difference between Fe and binary Fe–Cr alloys. Unfortunately, there is no data at higher dose in Fe for a full comparison.

3.2. Mechanical properties

Tensile tests have been performed in the temperature range from −160 °C to 300 °C, to determine if the model alloys exhibit a plastic instability similar to what has been observed in some ferritic–martensitic steels [21,28]. Engineering stress–strain curves for the four model alloys before irradiation and after irradiation to the three doses investigated in this work and tested at RT are shown in Fig. 9. The stress–strain curves clearly show irradiation hardening, increase of yield and ultimate tensile strength, as well as reduction of uniform and total elongation as compared to Fig. 3. The presence of Cr strongly influences radiation-induced

Table 2
Summary of size and density of the defect clusters determined in the investigated model alloys and irradiation doses

Dose	0.06 dpa		0.6 dpa		1.5 dpa	
Materials	Size (nm)	Density $10^{21}/m^3$	Size (nm)	Density $10^{21}/m^3$	Size (nm)	Density $10^{21}/m^3$
2.5Cr	8	1.2	13	2.7	16	2.2
5Cr	7	1.4	8	2.4	10	2.1
9Cr	6	1.3	7	1.9	13	1.7
uhp 9Cr	6	0.6	–	–	–	–
12Cr	–	–	6	1.7	6	1.7

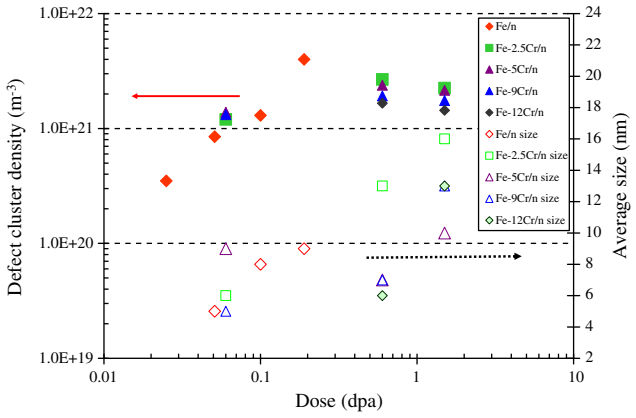

Fig. 8. Dose dependence of the defect density (open symbols) and size distribution (closed symbols) in Fe and Fe–Cr alloys.

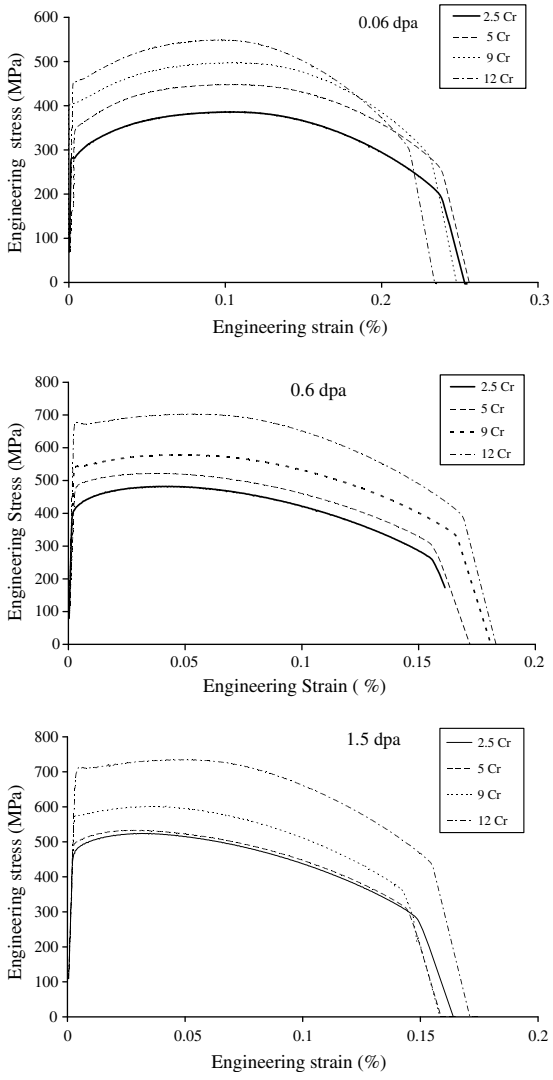

Fig. 9. Tensile tests at RT of model alloys before irradiation and for 0.06, 0.6 and 1.5 dpa.

hardening. At higher doses of irradiation, a slight decrease in work hardening is observed. Fig. 10 shows the variation of the yield stress as function of temperature at each dose. It demonstrates that the tensile strength increases with dose with the same amount independent of the testing temperature. They follow the same trend and all curves could be fitted using the same parameters for $\sigma_0 = 76$ MPa and $\beta = -0.0127$. Fig. 11, where the increase of the yield strength is plotted against the square root of the irradiation dose (for clarity), shows that model alloys harden more than Fe and saturate at a higher dose when compared to the behavior Fe irradiated under similar conditions. The yield strength dependence with doses shows that the addition of Cr enhances radiation-induced hardening. A small amount of Cr would increase the hardening drastically but the addition of about 9%Cr seems to moderate this increase, as it can be seen in Fig. 12, where a minimum hardening is found at around 9%Cr. Further, it can also be seen that in all Fe–Cr alloys the hardening continues to increase with dose, up to the highest one (1.5 dpa), in contrast to what has been observed in pure Fe [29], but similar to what has been found in F/M steels when irradiated under the same conditions [21]. This finding can be explained if the loops are considered to be of self interstitial atom (SIA) type and are responsible for hardening by their strong binding energy to Cr.

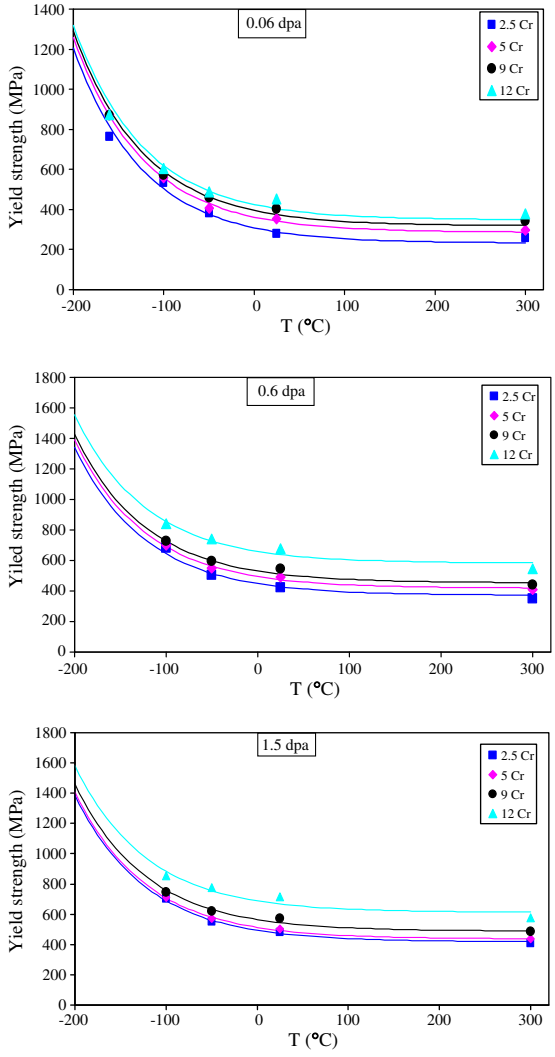

Fig. 10. Yield strength dependance on temperature for model alloys following irradiation to 0.06, 0.6 and 1.5 dpa.

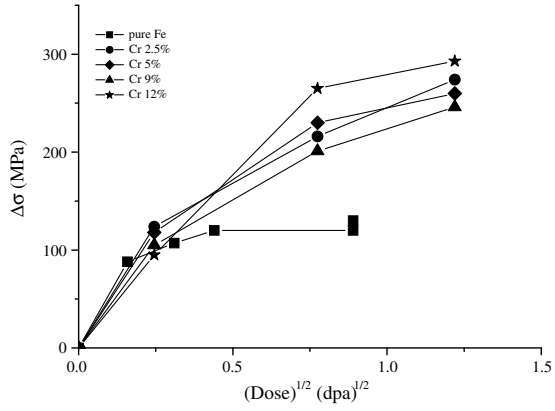

Fig. 11. Increase in room temperature yield strength upon irradiation at 300 °C, $\Delta\sigma_y$, vs $(\text{dose})^{1/2}$.

4. Discussion

Hardening mechanisms have been studied by correlating microstructural observations from TEM to mechanical property measurements using an Orowan-type mechanism. The Orowan model is an important contribution to the theory of yield stress of alloys containing non-shearable particles. The mechanism of how the particles could be by-passed is described in [30]. The evaluation of the by-passing stress was obtained by taking into account the influence of the dislocation character (edge or screw) on the equilibrium shape of the loop and interaction of the two arms of the dislocation on opposite sides of the loop. Strong obstacles, such as particles larger than 20 nm, do not release the dislocation before an Orowan loop is formed. But weaker obstacles such as solute atoms may release the dislocation at a larger angle. The Orowan model is given by the following equation:

$$\Delta\sigma_y = M\alpha\mu b(Nd)^{1/2}, \tag{3}$$

where Taylor coefficient: $M = 3.06$ [31], $\alpha = 0$–1 [32] and represents the strength of obstacles, Shear modulus: $\mu = 8.3 \times 10^4$ MPa [33], and the Burgers vector: $b = 0.248$ nm, N = density of defects and d is the defect size. This mechanism is applied here with the assumption that the radiation-induced defects are the 'only' defects that might hinder/slow down the movement of dislocations at the yield

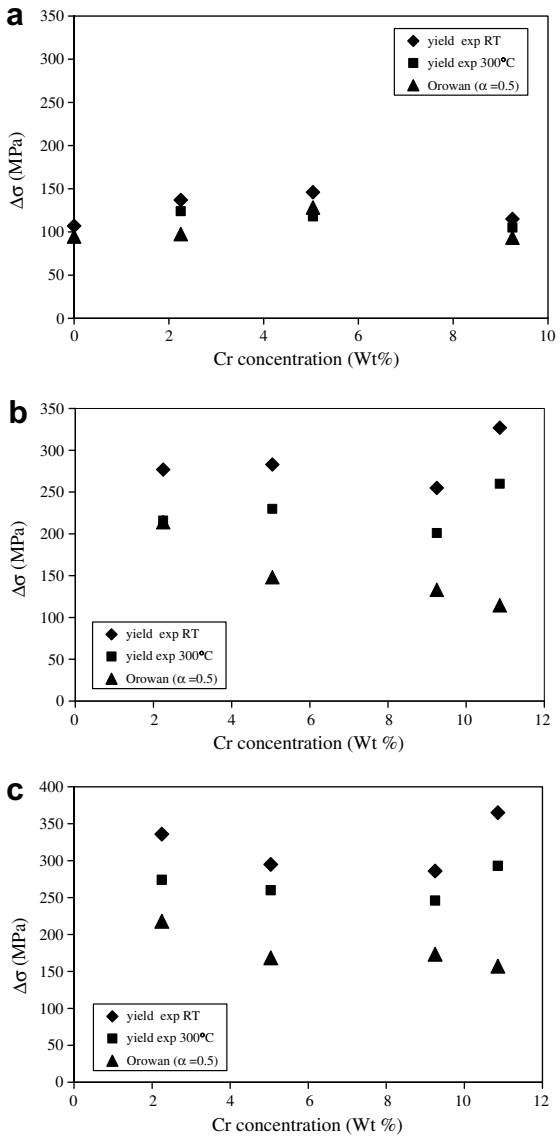

Fig. 12. Predicted hardening estimated from Eq. (3) (see text) compared to the measured hardening at RT and 300 °C as a function of Cr concentration after irradiation to (a) 0.06 dpa and (b) 1.5 dpa.

point during a macroscopic tensile test. As it will be shown later in this section, this assumption is rather rough but it allows a simple rationalization on how the observed microstructure affects the mechanical properties of a material and this from an experimental view point. To apply Eq. (3) to all investigated alloys, first the value of α is chosen to obtain the best agreement between the experimental results and the estimated values from Eq. (3), for the lowest dose of irradiation case. In fact, one single value of α (equal to 0.5) could be found to reach this agreement (Fig. 12(a)), which clearly indicates that the loops are the main features contributing to $\Delta\sigma$ at this dose. Then, the value of α was kept constant and used in Eq. (3) to estimate the hardening for all materials and doses of irradiation investigated here. At higher doses (Fig. 12(b) and (c)), it can be seen that the visible loops cannot be the only defects responsible for the measured irradiation-induced hardening, if the same value of α is used. In fact, the hardening predicted by Orowan mechanism decreases at higher doses, while hardening measured by tensile tests at both tested temperatures increases with dose and Cr concentration. A relative minimum is found around 9%Cr. Thus, the visible microstructure cannot account, in FeCr, for the measured hardening, which is larger than in Fe [29] at high enough dose (the density of visible defects, mainly dislocation loops, remains essentially constant, whereas the hardening increases with dose and has a non-monotonic dependence on Cr content) can be explained by either supposing that a larger density of hardening, but invisible defects are accumulated in FeCr compared to Fe and/or that the visible defects have a different strength with respect to the motion of dislocations in FeCr than in Fe. The former effect can be qualitatively understood if, with increasing dose, a large number of small clusters stabilised by Cr remain below the resolution of the electron microscope. The latter effect may, on the other hand, be related with a different proportion of $\langle 100\rangle$ and $1/2\langle 111\rangle$ dislocation loops depending on Cr concentration [34] and with the fact that $1/2\langle 111\rangle$ dislocation loops are more effective barriers to dislocation slip than $\langle 100\rangle$ loops [35]. In addition, above ~9%Cr the formation of α' precipitates enhanced by irradiation is expected [36,37]. These precipitates, coherent with the matrix, are hardly visible for the electron microscope, unless they reach large enough sizes, but they are certainly expected to contribute to hardening. On the other hand, the above-mentioned tendency to order, that appears below ~9%Cr under irradiation [36], may also influence the mechanical response of the material. A simplified, mechanistic approach can be hence proposed, whereby the radiation-hardening, $\Delta\sigma_y$, in FeCr would be the result of the composition of different contributions:

$$\Delta\sigma_y(\mathrm{FeCr}) = \Delta\sigma_y(\mathrm{Fe}) + \Delta\sigma_y^{\mathrm{SRO}} + \Delta\sigma_y^{\mathrm{invisible}} + \Delta\sigma_y^{\langle 111\rangle/\langle 100\rangle}. \quad (4)$$

Here, $\Delta\sigma_y$(Fe) represents the hardening in pure Fe, which saturates at relatively low dose and remains, afterwards, essentially constant. The other three terms correspond to phenomena that only occur in the presence of Cr and at higher doses, namely: short-range order parameter changes ($\Delta\sigma_y^{\mathrm{SRO}}$), allowing for either ordering or clustering (α'), depending on concentration; accumulation of invisible defects ($\Delta\sigma_y^{\mathrm{invisible}}$), most likely small interstitial clusters; and, finally, effect of a different ratio of $\langle 100\rangle$-to-$1/2\langle 111\rangle$ loops ($\Delta\sigma_y^{\langle 111\rangle/\langle 100\rangle}$), a term that could also include the effect of possible changes in the average size of the visible loops depending on Cr concentration, independently of the type. Precise investigations are needed to confirm or reject these contentions.

5. Conclusion

In this work, the effect of dose and Cr concentration on the mechanical properties and microstructure of model Fe alloys have been reported.

It was shown that the microstructure did not change after irradiation apart from the formation of radiation-induced dislocation loops. The size of cluster loops increases with dose, but decreases with Cr concentration. The density of the defect clusters increases with dose up to 0.6 dpa, but tends to saturate at higher doses. Both types of loops $a\langle 100\rangle$ and $a/2\langle 111\rangle$, are observed. However it is difficult to do quantitative analysis about the proportion of both types, which would be useful for modeling, as there is not enough statistics for this confirmation.

The nature of defects was also not definitively established from this examination.

For the mechanical properties, it is clearly shown that the presence of Cr strongly influences hardening vs dose:

- Hardening is much higher in all Fe–Cr alloys tested than in pure Fe.
- Hardening vs dose is similar in all Fe–Cr alloys up to 9%Cr. A higher hardening rate is observed for the Fe–12Cr alloy. A relative minimum is found around 9%Cr when the irradiation dose is high enough. This finding is believed to be due to the tendency to the short-range ordering of FeCr alloys when Cr concentration is below 9% and to the appearance of α' above this value. Thus, only the alloys having around 9%Cr are a random solid solution where a pure solute hardening mechanism could operate in addition to the effect of loops.

The Orowan-type of mechanism appears to be not appropriate to estimate the hardening from the TEM observed microstructure.

Acknowledgments

The authors would like to acknowledge the help of Metallurgy Department of Gent University for providing the model alloys, OCAS of Arcelor group/Belgium for their chemical analysis and Dr R. Lardé of the University of Rouen/France for the resistivity measurements. Special thanks to our colleagues of the mechanical and microstructure groups of NMS at LHMA, for their assistance and help during experiments, and also the technology department for the development and fabrication of the radiation rig. This work has benefited a lot from the simulating discussions and encouragements that we have received from Dr M. Jenkins (U-Oxford/UK) Dr M. Hernández-Mayoral (CIEMAT/Spain) and our colleagues Drs L. Malerba, E. Lucon, W. van Renterghem and M. Decréton.

This work was partially funded by the European Fusion Development Agreement under TTMS-007 task.

References

[1] R.L. Klueh, D.R. Harries, High-Chromium Ferritic and Martensitic Steels for Nuclear Applications, ASTM, 2001.
[2] H. Aït Abderrahim, Nucl. Instrum. and Meth. A 463 (2001) 487.
[3] K. Ehrlich, Fus. Eng Des. 56&57 (2001) 71.
[4] J. Van den Bosch, D. Sapundiev, A. Almazouzi, J. Nucl. Mater. 356 (2006) 237.
[5] E. Little, D. Stow, J. Nucl. Mater. 87 (1979) 25.
[6] T. Yamamoto, G.R. Odette, H. Kishimoto, J.W. Rensman, P. Miao, J. Nucl. Mater. 356 (2006) 27.
[7] D. Sapundjiev, S. Van Dyck, W. Bogaerts, Corros. Sci. 48 (2006) 577.
[8] C.E. Webb, J. Iron Steels Inst. 124 (1931) 141.
[9] R.M. Bozorth Ferromagnetism, Van Norstand, Princeton, NJ, in: K. Schröder (Ed.), CRC Handbook of Electrical Resistivities of Binary Metallic Alloys, CRC Press, Inc., Boca Raton, Florida, 1951.
[10] P. Olsson, Phys. Rev. B 73 (2006) 104416.
[11] D. Terentyev, L. Malerba, A.V. Barashev, Philos. Mag. Lett. 85 (2005) 587.
[12] N. Yoshida, A. Yamaguchi, T. Muroga, Y. Miyamoto, K. Kitajima, J. Nucl. Mater. 155–157 (1988) 1232.
[13] S.I. Porollo, J. Nucl. Mater. 256 (1998) 247.
[14] K. Arakawa, M. Hatanaka, H. Mori, K. Ono, J. Nucl. Mater. 329–333 (1988) 1232.
[15] A. Kohyama, A. Hishinuma, D.S. Gelles, J. Nucl. Mater. 233–237 (1996) 138.
[16] K. Shiba, M. Enoeda, S. Jitsukawa, J. Nucl. Mater. 329–333 (2004) 243.
[17] M. Matijasevic, A. Almazouzi, SCK·CEN-R-4196, 2005.
[18] F. Maury, P. Lucasson, A. Lucasson, F. Faudot, J. Bigot, J. Phys. F: Met. Phys. 17 (1987) 1143.
[19] C. Dimitrov, A. Benkaddour, C. Corbel, P. Moser, Ann. Chim. Fr. 16 (1991) 319.
[20] V. Jaquet, Thesis de Docteur de l'école polytechnique de Paris, France, 2000.

[21] M. Matjasevic, E. Lucon, A. Almazouzi, J. Nucl. Mater., these Proceedings.
[22] G.E. Dieter, Mech. Metall. (1986).
[23] M. Weber, MIRE-CR-irradiation report, NT.57/F040112/0/MW/MM/AA.rw, SCK-CEN internal report'2004.
[24] M. Matijasevic, A. Almazouzi, SCK·CEN-R-4472, May 2007.
[25] M.L. Jenkins, M.A. Kirk, Characterisation of Radiation Damage by Transmission Electron Microscopy, Institute of Physics Series in Microscopy in Materials Science, 2001.
[26] M. Matijasevic, W. van Rentenghem, A. Almazouzi (in press).
[27] M. Hernández-Mayoral, Private communication.
[28] A.F. Rowcliffe, J.P. Robertson, R.L. Klueh, K. Shiba, D.J. Alexander, M.L. Grossbeck, S. Jitsukawa, J. Nucl. Mater. 258–263 (1998) 1275.
[29] K. Verheyen, M. Jardin, A. Almazouzi, J. Nucl. Mater. 351 (2006) 209.
[30] R.M. Thomson, in: R.W. Cahn, P. Haasen (Eds.), Physical Metallurgy, fourth ed., North-Holland, 1996.
[31] R.E. Stoller, S.J. Zinkle, J. Nucl. Mater. 283–287 (2000) 349.
[32] D. Hull, D.J. Bacon, Introduction to Dislocations, fourth ed., Butterworth and Heinmann, Oxford, 2001.
[33] G. Gosh, G.B. Orson, Acta Mater. 50 (2002) 2655.
[34] D.S. Gelles, J. Nucl. Mater. 108&109 (1982) 515;
D.S. Gelles, J. Nucl. Mater. 225 (1995) 163.
[35] D.S. Gelles, R. Schäublin, Mater. Sci. Eng. A 309&310 (2001) 82.
[36] N.P. Filippova, V.A. Shabashov, A.L. Nikolaev, Phys. Met. Metall. 90 (2000) 145.
[37] M.H. Mathon, Y. De Carlan, G. Geoffroy, X. Averty, A. Alamo, C.H. de Novion, J. Nucl. Mater. 312 (2003) 236.